RESEARCH ARTICLE

Open Access

Assessing the impact of climate change on sediment discharge using a large ensemble rainfall dataset in Pekerebetsu River basin, Hokkaido

Riho Kido[1], Takuya Inoue[1*], Misako Hatono[1] and Kazuki Yamanoi[2]

Abstract

Increased rainfall associated with climate change can increase sediment discharge. The supply of fine sediment from slope failures inhibits bed armoring of mountain rivers and increases sediment discharge to the downstream reaches. Floods without slope failures lead to bed erosion and armoring and may ultimately decrease sediment discharge. Thus, it is important to consider sediment discharge from slope failure and bed erosion as factors affecting sediment production. Climate change affects not only the rainfall amount, but also the temporal rainfall pattern; consequently, the pattern affects the sediment production factors and the amount of sediment discharge. However, changes in sediment discharge due to climate change based on sediment production sources have not yet been clarified. In this study, we statistically analyzed 1200 results simulated using a physics-based sediment runoff model to assess the impact of changes in temporal rainfall patterns on sediment discharge and sediment production sources in the Pekerebetsu River Basin. In the simulations, we used the rainfall predicted in d4PDF (Database for policy decision-making for future climate change), a large ensemble climate simulation database at 5 km and 20 km resolutions. Our results showed that the climate-driven increase in sediment discharge was considerably larger than that of rainfall. An increase in short-term heavy rainfall increased the supply of fine sediments from slope failure. This resulted in the suppression of bed armoring and a large increase in sediment discharge. Thus, the increase in sediment discharge is not only caused by an increase in rainfall but also by changes in temporal rainfall patterns and sediment production factors. The sediment discharge calculated for the 20 km resolution climate projection was nearly one order of magnitude smaller than that for the 5 km resolution. This suggests that the 20 km resolution climate projections do not adequately represent orographic rainfall in the mountains and thus, do not adequately reproduce extreme sediment discharge events. An increased sediment supply causes bed aggradation and decreases the river conveyance capacity of the downstream channel. The model developed in this study will contribute to flood risk analysis and flood control planning for increased rainfall due to climate change.

Keywords Climate change, Sediment discharge, Large-ensemble data, Temporal rainfall pattern, Slope failure, Channel erosion, Spatial resolution of climate change projections

*Correspondence:
Takuya Inoue
inouetakuya@hiroshima-u.ac.jp
[1] Graduate School of Advanced Science and Engineering, Hiroshima University, 1-4-1 Kagamiyama, Higashi-Hiroshima, Hiroshima 739-8527, Japan
[2] Disaster Prevention Research Institute, Kyoto University, Kyoto 612-8235, Japan

1 Introduction

The recent increase in flooding worldwide has been attributed to atmospheric factors; however, an often-forgotten factor is the reduction in river conveyance capacity associated with sediment deposition (Lane et al. 2007; Sofia and Nikolopoulos 2020; Milan and Schwendel 2021). Changes in river conveyance capacity do not affect the amount of water that flows through the river system during a flood, but they affect the probability of a flood event overtopping the embankments and flood defenses. Increased sediment supply can contribute to bank erosion in gravel beds (Métivier et al. 2017; Ahmed et al. 2019; Inoue et al. 2020; Rachelly et al. 2022) and sediment-induced abrasion in bedrock rivers (Sklar and Dietrich 2004; Inoue and Nelson 2020; Inoue et al. 2021), resulting in bridge failures. In addition, an increasing number of towns located in valleys and fans are affected by flooding, including debris flows, in countries with steep mountains such as Japan and Switzerland (Rickenmann and Koschni 2010; Shimizu et al. 2020; Hashimoto et al. 2020).

Simulations using General Circulation Models (GCMs) predict increased rainfall intensity in many parts of the world under most future climate change scenarios, and it is generally believed that such increased rainfall intensity will lead to increased landslide activity (Crozier 2010; IPCC 2021). However, there is still a high level of uncertainty due to the errors inherent in scenario-driven world predictions and the coarse spatial resolution of currently available downscaled predictions (Crozier 2010). Recently, model development aimed at simulating large-scale sediment transport in GCMs has become active (Hatono and Yoshimura 2020; Li et al. 2022; Cohen et al. 2022). Several studies have incorporated global and regional climate models into physics-based slope-stability models to investigate the effects of climate change on landslides (Ciabatta et al. 2016; Alvioli et al. 2018; Peres and Cancelliere 2018; Hürlimann et al. 2022). However, it remains unclear how the spatial resolution of climate change projection models affects sediment runoff.

Landslides are not the only sources of sediment transported to rivers and towns located in valleys and fans. In a 2016 flood event in Hokkaido, Japan, Miyazaki et al. (2018) and Furuichi et al. (2018) conducted field observations and found that 70 % of the sediment discharged from the upper reaches of the Pekerebetsu River, a tributary of the Tokachi River located in eastern Hokkaido, into the downstream fan originated from the riverbed of the upstream mountainous river. Higher rainfall increases the flow rate of mountain rivers, consequently increasing their sediment transport capacity (Hürlimann et al. 2022). In addition, riverbed deformation in mountain rivers can alter the grain size distribution of sediments in the riverbed and cause phenomena that affect sediment transport rates, such as armoring (e.g., Pitlick et al. 2008). However, the effects of climate change on the sediment transport capacity and grain size in mountain rivers remain largely unknown.

In this study, we investigated changes in sediment discharge due to climate change using a large ensemble climate simulation database (d4PDF; Mizuta et al 2017; Ishii and Mori 2020) as input to a physics-based model that accounts for landslides, mountainous channel erosion, and grain size changes. We also clarified the effect of the spatial resolution of d4PDF (Yamada et al. 2018) on sediment discharge. Furthermore, we calculated the sediment discharge derived from each production source and determined how changes in temporal rainfall patterns caused by climate change affect sediment production and runoff.

2 Methods

2.1 Study area

Our study area was the upper reaches of the Pekerebetsu River in Hokkaido, Japan (Fig. 1a). The Pekerebetsu River is a tributary of the Tokachi River that flows into the Pacific Ocean. The Tokachi River is located in a cold region (Peel et al. 2007). The annual precipitation averaged from 1996 to 2005 in the Tokachi River Basin was approximately 900 mm, which is much less than the average annual precipitation of 1600 mm for other basins in Japan (River Bureau and Ministry of Land, Infrastructure, Transport, and Tourism 2006). However, in late August 2016, heavy rains due to fronts and typhoons caused river overflows and landslides, mainly in the Tokachi River Basin, resulting in extensive damage in many areas (Fig. 1b). Warm moisture carried by typhoons developed into orographic rainfall near our study site and became the heaviest rainfall in Hokkaido since observations began in 1977, exceeding 500 mm in three days centered in the Hidaka Mountains (Aoki et al. 2018).

The upper reaches of the Pekerebetsu River consist mainly of granite, which is easily weathered. The periglacial deposits formed by repeated freezing and thawing of the bedrock during the glacial period were distributed in the surface layer of the slopes at the bottom of the valley (Miyazaki et al. 2018). As mentioned above, these sediments remain on the slopes and mountainous riverbeds because there is generally little rainfall in this watershed, and large amounts of sediment are easily runoff downstream once heavy rains occur. The peak flow discharge at the downstream end of the study area was 402 m^3/s (Hokkaido Torrential Rainfall Hazard Research Team 2017), and the total amount of sediment discharged from the study site was 380,800 m^3 which was estimated from the difference in LiDAR surveys across this event
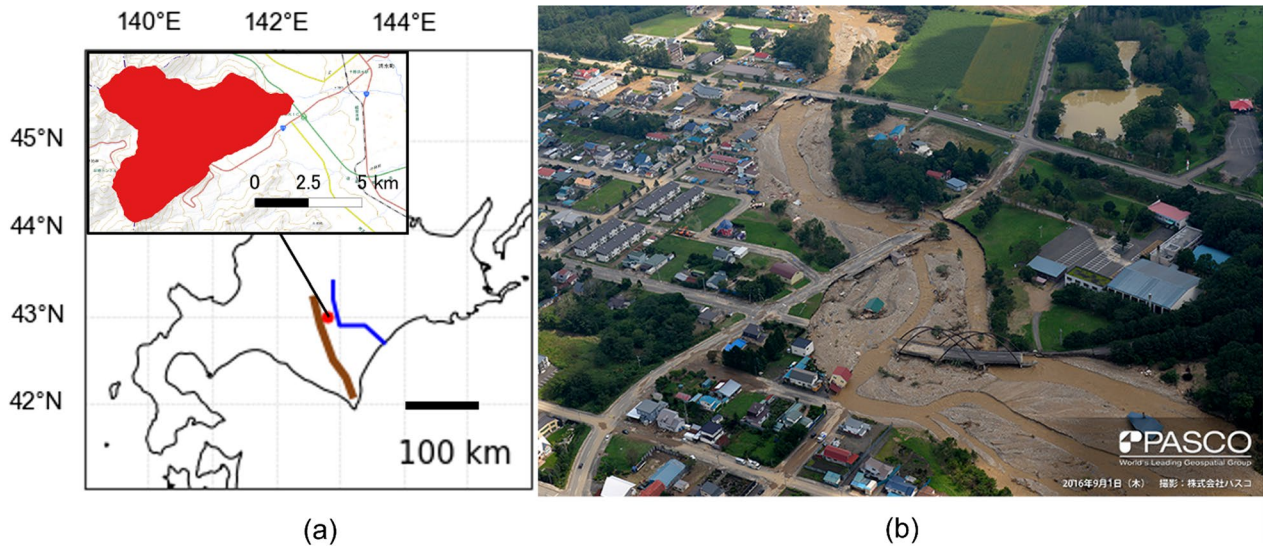
Fig. 1 Information of study area. **a** Map of Hokkaido Island (Japan) and location of Pekerebetsu River basin, Hokkaido, Japan. The red area is the study area, the blue line is the Tokachi River, the brown line is the Hidaka Mountains. **b** Aerial photograph of the flooding including debris flow at Pekerebetsu River after 2016 heavy rainfall (Taken on September 1, 2016)

(Ministry of Land, Infrastructure, Transport and Tourism 2017). In addition, Miyazaki et al. (2018) stated that 70% of the sediment was produced from the riverbed.

2.2 Model

2.2.1 Model summary

In this study, we used a numerical model (see Additional file 1) to assess the effects of climate change on sediment discharge. This model comprises three physics-based components: First, the sediment production model calculates the amount of sediment produced by slope failure. Based on Darcy's law, slope failure occurs when the amount of water in the soil exceeds a threshold. Second, the sediment supply model calculates the amount of sediment supplied from the slopes to the river channels. Sediment is supplied to a river channel when it exceeds the amount deposited on a cliff cone. Third, the sediment transport model calculates the bed-load and suspended-load transport rates that flow through the channel accompanied by the erosion and deposition of the riverbed. Here, we defined the sediment discharge as the sum of the bedload and suspended load transport rates at the downstream end of the study site. The bedload and suspended-load transport rates were mainly controlled by the Shields number ($\tau_* = hI/sd$), which was calculated using the flow depth and velocity from a kinematic wave model, where, h is the water depth, I is the energy slope, s is the specific gravity of the submerged sediment, and d is the grain size of the sediment. The flow discharge required for depth and velocity simulations was determined by the runoff model (Wooding 1965) using

rainfall data and was provided as input to each channel reach.

2.2.2 Model modification

In this study, we investigated how predicted future climate change will alter the balance between sediments produced from slopes and riverbeds. We modified the sediment mass conservation law using the method proposed by Inoue et al. (2020) to track sediments based on production sources, as follows:

$$
\begin{aligned}
(1-\lambda)\frac{\partial z_b^i}{\partial t} = \frac{1}{B^i}\Bigg(& \sum_{k=1}^{n_k} Q_{b_k}^{u1_{i,j=1}} + \sum_{k=1}^{n_k} Q_{b_k}^{u2_{i,j=1}} - \sum_{k=1}^{n_k} Q_{b_k}^{i,j=1} \\
& + \sum_{k=1}^{n_k} Q^{u1_i} c_k^{u1_{i,j=1}} + \sum_{k=1}^{n_k} Q^{u2_i} c_k^{u2_{i,j=1}} - \sum_{k=1}^{n_k} Q^i c_k^{i,j=1} \\
& + \sum_{k=1}^{n_k} Q_{b_k}^{u1_{i,j=2}} + \sum_{k=1}^{n_k} Q_{b_k}^{u2_{i,j=2}} - \sum_{k=1}^{n_k} Q_{b_k}^{i,j=2} \\
& + \sum_{k=1}^{n_k} Q^{u1_i} c_k^{u1_{i,j=2}} + \sum_{k=1}^{n_k} Q^{u2_i} c_k^{u2_{i,j=2}} - \sum_{k=1}^{n_k} Q^i c_k^{i,j=2} \\
& + \sum_{k=1}^{n_k} Q_{sup_k}^{Li} + \sum_{k=1}^{n_k} Q_{sup_k}^{Ri} \Bigg)
\end{aligned}
$$

(1)

where λ is the porosity of riverbed materials, z_b is the riverbed elevation, B is the width, Q is the water discharge, Q_{b_k}, c_k, Q_{sup_k} are, respectively, the bed load discharge, concentration of the suspended load, and supplied sediment discharge of the material with k grain size. The superscript indicates the ID of the unit channels; i

Kido *et al. Progress in Earth and Planetary Science* (2023) 10:54

Page 4 of 14

,$u1_i$, and $u2_i$ indicate the unit channel i, and the two upstream channels connected to it. The superscripts L_i and R_i indicate the ID of the unit slopes located on the left and right sides of the unit channel i, respectively. j indicates the identification number of each production source ($j = 1$: riverbed; $j = 2$: slope).

In our model, we used Ashida and Michiue's equation (Ashida et al. 1991) and the modified Egiazarov equation (Ashida et al. 1991) to estimate the bedload transport rate and critical Shields number (i.e., Shields number at the threshold for sediment motion). In addition, we used Itakura and Kishi's equation (1980) and Rubey's equation (Rubey 1933) to estimate the entrainment and deposition rates of the suspended loads, respectively.

2.2.3 Parameter input and calibration

We generated geometric input data of slopes and channels from a DEM with 10 m resolution measured by LiDAR prior to the flood published by the Geospatial Information Authority of Japan. Miyazaki et al. (2018) investigated the grain size distribution at terraces and cliff cones that remained uneroded after the 2016 heavy rainfall (Fig. 2). They investigated the grain size distribution by measuring the triaxial and weight in the field for gravels larger than 75 mm in grain size and by conducting laboratory tests for sand and gravel smaller than 75 mm in grain size. To calculate the sediment discharge, we used the average grain size distribution of the terrace deposits for the initial riverbed materials and that of the cliff cone deposits for the slope failure materials. In addition, the coefficient of permeability was set to 0.0001 m/s, based on Creager 's Table (1945), which was estimated from the grain sizes at which 20 percent of the total weight was finer.
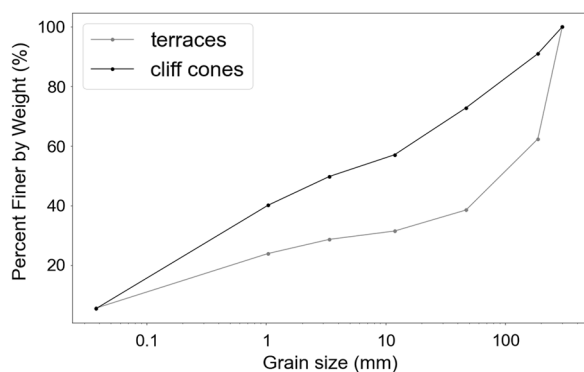

Fig. 2 Grainsize distribution of study area observed by Miyazaki et al (2018) after the 2016 heavy rainfall. Black symbols show the average values collected from river terraces which were not eroded during 2016 heavy rainfall, and gray symbols show the averages value collected from cliff cones which deposited during 2016 heavy rainfall

To reproduce observed values during the 2016 heavy rainfall (see Sect. 2), we calibrated the model parameters (i.e., α_c, γ and f). For the input rainfall data, we used the AMeDAS rainfall data from July 1 to September 5, including the heavy rainfall of 2016. Here, α_c is a parameter for setting the channel width based on the regime law ($\alpha_c = 5$) and γ is a parameter that corrects for the thresholds of slope failure ($\gamma = 0.91$). Also, f is the infiltration rate into the bedrock under the soil layer ($f = 0.01$ mm/h) and we set a very small value because the bedrock infiltration is not dominant during heavy rain (see the Additional file 1).

Comparing the calculated results with the observed results, the peak flow discharge was 397 m^3/s in the calculated results compared to 401 m^3/s in the observed results. The total sediment volume that flowed out of the basin was 387,000 m^3 in the calculated results, compared to 380,800 m^3 in the observed results. The percentage of sediment produced from the slope was 33% in the calculated results compared to 30% in the observed results. Thus, our model accurately captured the flow and sediment discharge observed in the study area.

3 Results
3.1 Rainfall data analysis

To evaluate extreme events that are statistically infrequent, we used a large ensemble data for climate change in Japan, called d4PDF (Mizuta et al 2017). The Database for Policy Decision Making for Future Climate Change (d4PDF) uses a global atmospheric model for historical climate simulation and +4 K future climate simulation with a 60 km resolution and the model for the area surrounding Japan with a 20 km resolution. In historical climate simulations, the sea surface temperature (SST) and greenhouse gas concentrations observed from 1951 to 2010, among others, were prescribed as boundary conditions. It contains 6000 years of data, with each of the 100 members calculated from different initial values and 60 years time perturbation. On the other hand, in the +4 K future climate simulation, the global average temperature increased by 4 °C compared to that before the Industrial Revolution in 1850. It contains 5400 years of data, with 60 years time perturbation for each of the 90 members that were given 15 perturbations representing observational uncertainties in six different warming patterns. Thus, this prediction was not made for a specific year, and there was no target period. The d4PDF of the area around Japan with a 20 km resolution is a dynamic downscaling of the global model. There were 3000 years of data for the historical climate simulation and 5400 years of data for the +4 K future climate simulation (Mizuta et al 2017). We extracted the data from this large ensemble dataset. First, a cumulative probability

density function based on the Gumbel distribution following Hoshino and Yamada (2023) is calculated using the annual maximum 3-day precipitation within a single 60-year ensemble member. This was performed for all members of the historical climate simulation and +4 K future climate simulation. Then, 10 members with various slopes in the cumulative probability density function were manually selected for each historical climate simulation and +4 K future climate simulation. This provided data for 600 years each for the historical climate simulation and the +4 K future climate simulation.

The spatial resolution of the d4PDF is 20 km, which does not accurately reproduce heavy orographic rainfall. Therefore, we also used rainfall data downscaled to a 5 km resolution by Yamada et al. (2018) as input in our model for comparison. We used the watershed average for the 5 km resolution and the rainfall of one grid containing the study area for a 20 km resolution. Because Yamada et al. (2018) only downscaled 10 days, which includes the timing of maximum rainfall in each year, we simulated 10 days' worth of sediment discharge for 600 years in the historical climate simulation and +4 K future climate simulation.

We computed the maximum annual rainfall and 10-day total rainfall return period using the extracted d4PDF rainfall data. We used a nonparametric method (Cunnane 1978) to calculate the return period.

$$P = \frac{N + 0.6 - i}{N + 0.2} \tag{2}$$

where P is the non-exceedance probability, N is the number of samples, and i is the number of ranks of the samples sorted by the order of magnitude.

The annual maximum rainfall increased by a factor of about 1.3 to 1.4 for the 20 km resolution and by a factor of about 1.4 to 1.6 for the 5 km resolution from historical climate simulation to +4 K future climate simulation (Figs. 3b, 3d, and Table 1), while the 10-day total rainfall increased by a factor of about 1.0–1.1 for the 20 km resolution and by a factor of 1.2–1.3 for the 5 km resolution (Fig. 3a, c, and Table 1). Thus, the annual maximum rainfall has a larger increase rate due to predicted climate change compared to the total rainfall, and the increase rates are larger at the 5 km resolution than those at the 20 km resolution in our study area.

To investigate the effects of temporal rainfall patterns on sediment runoff, we conducted a cluster analysis on the d4PDF hyetograph. First, we extracted data 60 h before and after the peak rainfall with a return period greater than 2 years and applied normalization so that the maximum rainfall was equal to 1. The obtained rainfall patterns were classified into six clusters using the k-means method (Macqueen 1967) (Fig. 4). The six

clusters were characterized, as shown in Table 2. Types 1 and 2 had short and long rainfall durations, respectively. Type F experienced heavy rainfall before the peak, Type M experienced heavy rainfall around the peak, and Type L experienced heavy rainfall after the peak. The heat map in Fig. 5 shows the classification ratio of all rainfall events that were clustered in the historical and +4 K future climate simulations. The historical climate simulation had more events with a maximum rainfall of 15 mm/h or less, whereas the +4 K future climate simulation had more events with larger maximum rainfall. In particular, short-term rainfall patterns (M-1 and L-1), with a maximum rainfall of 25 mm/h or more, are increasing.

3.2 Climate change impact

A comparison between Figs. 3 and 6 and Tables 1 and 3 shows that the increased rate of sediment discharge at both resolutions was larger than those of annual maximum rainfall and 10-day total rainfall. Thus, we analyzed the factors that contributed to the increase in sediment discharge in detail by focusing on the results from the 5 km resolution where the sediment increase was particularly large. In other words, why did sediment discharge increase 3–5.5 times while precipitation increased only 1.2–1.6 times and flow discharge increased only 1.6–1.9 times? Because flow discharge is linked to rainfall, the rapid increase in sediment discharge cannot be explained solely by an increase in stream bed stress due to increased flow discharge.

The heat map in Fig. 7 shows the proportion of sediment produced from the slope. The vertical and horizontal axes were delimited in the same manner, as shown in Fig. 5. As mentioned in Sect. 4, climate change increases the number of short-term rainfall patterns (M-1 and L-1) with a maximum rainfall of 25 mm/h or more. When the maximum rainfall was greater than 25 mm/h, the proportion of sediment produced from the slopes was higher in short-term rainfall patterns. This suggests that when the maximum rainfall is high, short-term rainfall increases slope failure.

Figure 8 shows the changes in the proportion of sediment produced from the slope (*Pslope*) and the average grain size of the exchange layer (*Fm*) at the end of each year. We can see that *Fm* is smaller when *Pslope* is larger, and vice versa, indicating that the average grain size of the exchange layer decreases as the slope failure increases. When fine sediments are fed into armored beds owing to slope failure, the friction angle between the bed materials decreases, and the critical Shields number for incipient sediment motion decreases (Egiazaroff 1965). Thus, even if the flow discharge was the same, the sediment on the riverbed moved more
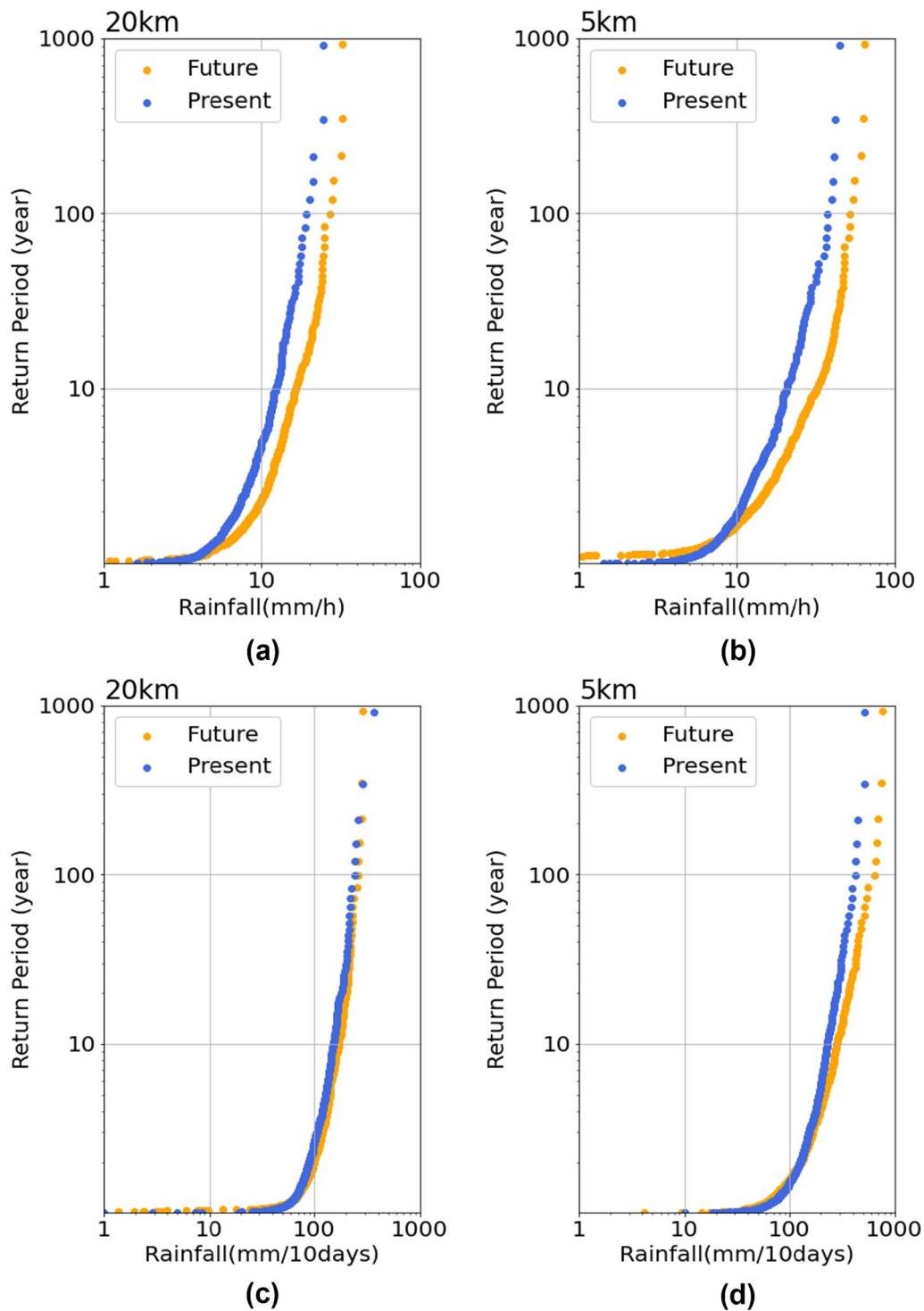
Fig. 3 Return periods for historical and +4 K future climate simulation rainfalls. **a** Annual maximum rainfall at 20 km resolution, **b** annual maximum rainfall at 5 km resolution, **c** 10-days total rainfall at 20 km resolution, and **d** 10-days total rainfall at 5 km resolution. Blue and orange dots represent historical climate simulation and +4 K future climate simulation, respectively

Table1 Comparison of rainfall for each return period

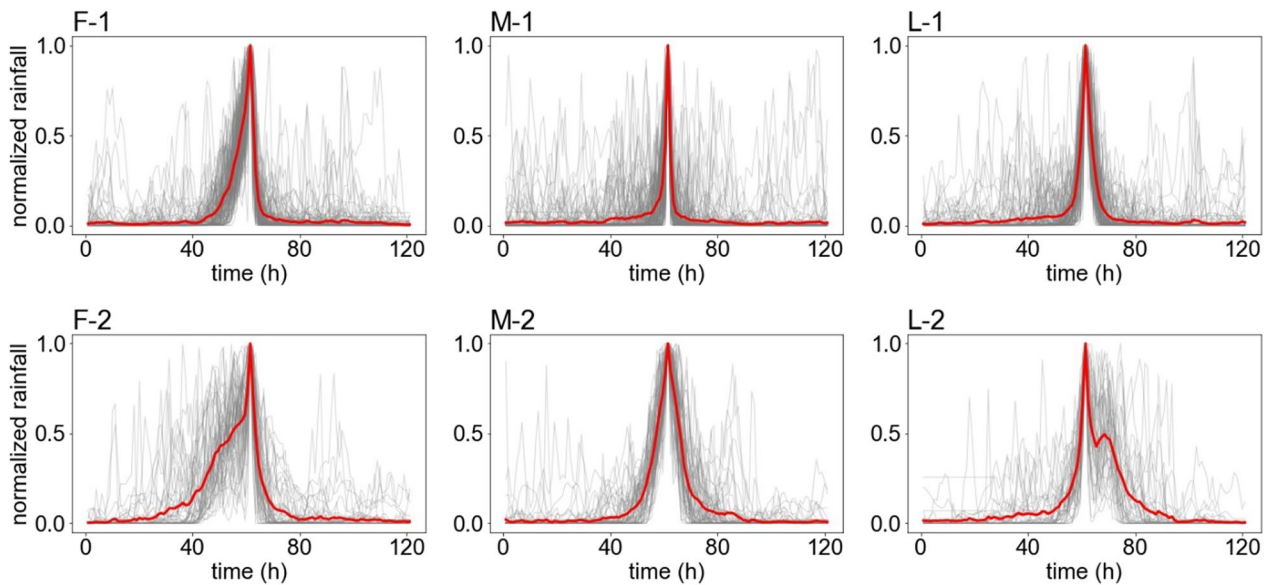| Return period	20 km			5 km		
	Present (P_{20})	Future (F_{20})	Ratio of increase (F_{20}/P_{20})	Present (P_5)	Future (F_5)	Ratio of increase (F_5/P_5)
Annual maximum rainfall (mm/h)						
50	17.3	24.3	1.40	33.5	47.7	1.42
20	14.2	20.6	1.45	25.8	41.2	1.60
10	12.3	16.6	1.35	20.0	32.2	1.61
Total rainfall (mm/10 days)						
50	213.7	224.9	1.05	353.7	477.3	1.35
20	179.0	201.0	1.12	280.4	365.4	1.30
10	152.5	168.8	1.11	229.4	275.0	1.20

Fig. 4 Rainfall patterns of historical and +4 K future climate simulation data clustered using k-means method. The gray lines represent the rainfall pattern for each year, and the red line represents the average of all years in each cluster

Table 2 Characteristics of rainfall patterns

	Heavy rainfall		
	Before the peak	Around the peak	After the peak
Rainfall duration			
Short	F-1	M-1	L-1
Long	F-2	M-2	L-2

easily. Increased water volume due to climate change flows over these non-armored beds, causing large amounts of sediment to run off. This may explain why the rate of increase in the sediment discharge was higher than the rate of increase in rainfall. A nonlinear relationship exists between rainfall, flow, and sediment discharge. Tan et al. (2021) predicted that increased extreme rainfall in the Mississippi/Atchafalaya River
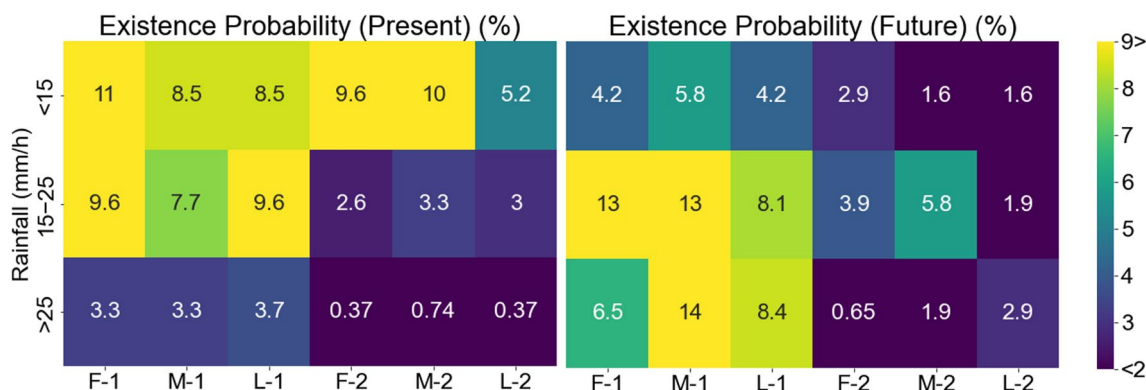
Fig. 5 Existence probability of rainfall. The horizontal axis represents the differences in rainfall patterns based on the clustering results shown in Fig. 4. The vertical axis represents the maximum rainfall by dividing it into three categories: 15 mm/h or less, more than 15 mm/h, and 25 mm/h or less, and more than 25 mm/h
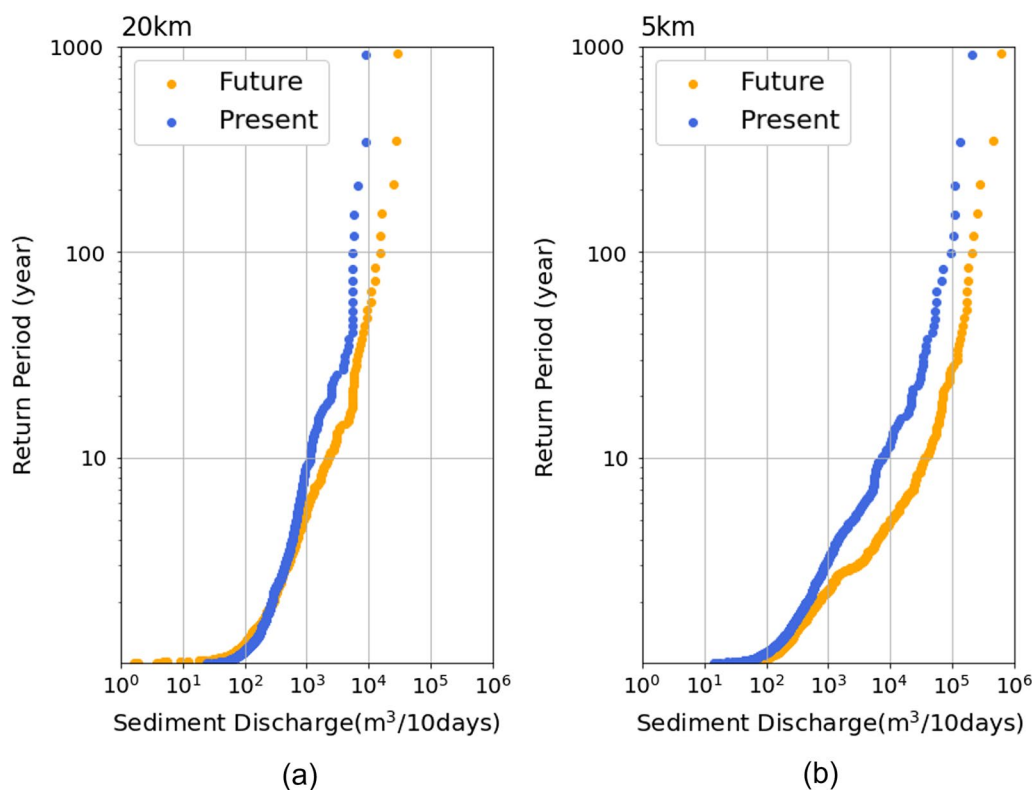

Fig. 6 Return period of the amount of sediment discharge for 10 days. **a** Results using 20 km resolution rainfall data, and **b** Results using 5 km resolution rainfall data. Blue and orange dots represent historical climate simulation and +4 K future climate simulation, respectively

Basin increases N and P fluxes owing to erosion and will continue to increase in the future owing to increased extreme rainfall events with climate change. Therefore, the rates of increase were different. However, the rate of increase in sediment discharge is considerably higher than the other rates of increase. The supply of

fine sediments from the slope contributed significantly to this result.

The average grain size of the exchange layer (*Fm*) was affected not only by *Pslope* but also by the timing of heavy rainfall. The heat map in Fig. 9 shows the average grain size of each type. For Type 1, there

Table3 Comparison of the flow and sediment discharge for each return period

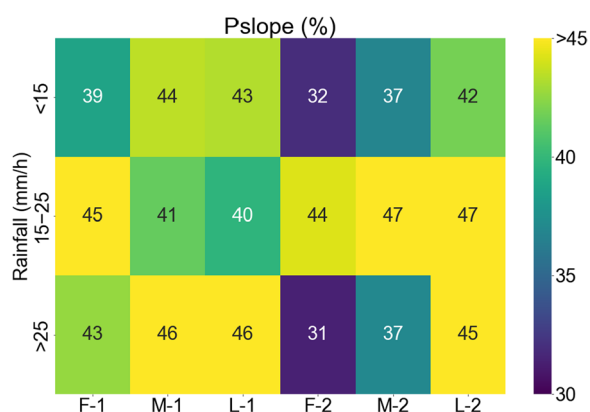| Return period	20 km			5 km		
	Present (P_{20})	Future (F_{20})	Ratio of increase (F_{20}/P_{20})	Present (P_5)	Future (F_5)	Ratio of increase (F_5/P_5)
Flow discharge (m³/s)						
50	77	48	1.60	241	148	1.62
20	56	42	1.31	183	107	1.70
10	47	30	1.57	136	71	1.91
Amount of sediment discharge (m³/10 days)						
50	5497	9288	1.69	52,107	152,833	2.93
20	2391	5560	2.32	23,965	87,747	3.66
10	1124	2218	1.97	7379	40,830	5.53

Fig. 7 The proportion of sediment produced from the slope averaged over all cases for each mesh. The horizontal axis represents the differences in rainfall patterns based on the clustering results shown in Fig. 4. The vertical axis represents the maximum rainfall by dividing it into three categories: 15 mm/h or less, more than 15 mm/h and 25 mm/h or less, and more than 25 mm/h

were no significant differences between F-1, M-1, and L-1 because of the short rainfall duration, whereas for Type 2, there were different trends for each rainfall rank. First, when the maximum rainfall was less than 15 mm/h, *Fm* of L-2 decreased. This is because the *Pslope* of L-2 was larger than that of F-2 and M-2, and the supply of fine sediment from the slope was large. When the maximum rainfall was between 15 and 25 mm/h, *Pslope* was almost the same for all types, but the timing of the heavy rainfall becomes later, *Fm* becomes larger. This is because as the timing of the heavy rainfall is delayed, fine sediments are discharged within the event, and armoring occurs after the event ends. Finally, when the maximum rainfall was greater than 25 mm/h, *Fm* was larger in L-2 than in F-2, although *Pslope* of L-2 was significantly larger than that

of F-2. When the maximum rainfall is large and there is heavy rainfall after the peak, even though there is a large supply of fine sediment from the slope, most of this is discharged during the event, and the grain size after the event becomes larger. As shown above, when the maximum rainfall was small, the average grain size decreased with the amount of fine sediment supplied from the slope; however, when the rainfall was large, the average grain size increased with the amount of rainfall after the peak.

3.3 Grid resolution impact

The 5-km resolution shows annual maximum rainfall and 10-day accumulated rainfall that are 1.5 to 2 times larger than those of the 20-km resolution (Table 4). However, the calculated sediment runoff from these rainfall events was considerably larger, by a factor of 10–20 from 20-km resolution to 5-km resolution (Table 4). Most of the rainfall events in the 20-km resolution had an annual maximum rainfall of 15 mm/h or less and did not represent the strong rainfall that was represented in the 5-km resolution (Table 5). Thus, the 20-km resolution may underestimate the amount of sediment discharge because it cannot represent rainfall strong enough to cause a large amount of sediment discharge.

In addition, as shown in Fig. 6, in the case of 20 km resolution, the 380,000 m³ sediment discharge observed during heavy rainfall in 2016 was not included in either the historical climate simulation results or the +4 K future climate simulation results. On the other hand, for the 5 km resolution, the maximum value of the current climate results is close to that value. Therefore, it is desirable to use rainfall data with a resolution that can represent strong rainfall to accurately predict the amount of sediment discharge in mountainous areas where heavy orographic rainfall is the main determinant of sediment runoff.
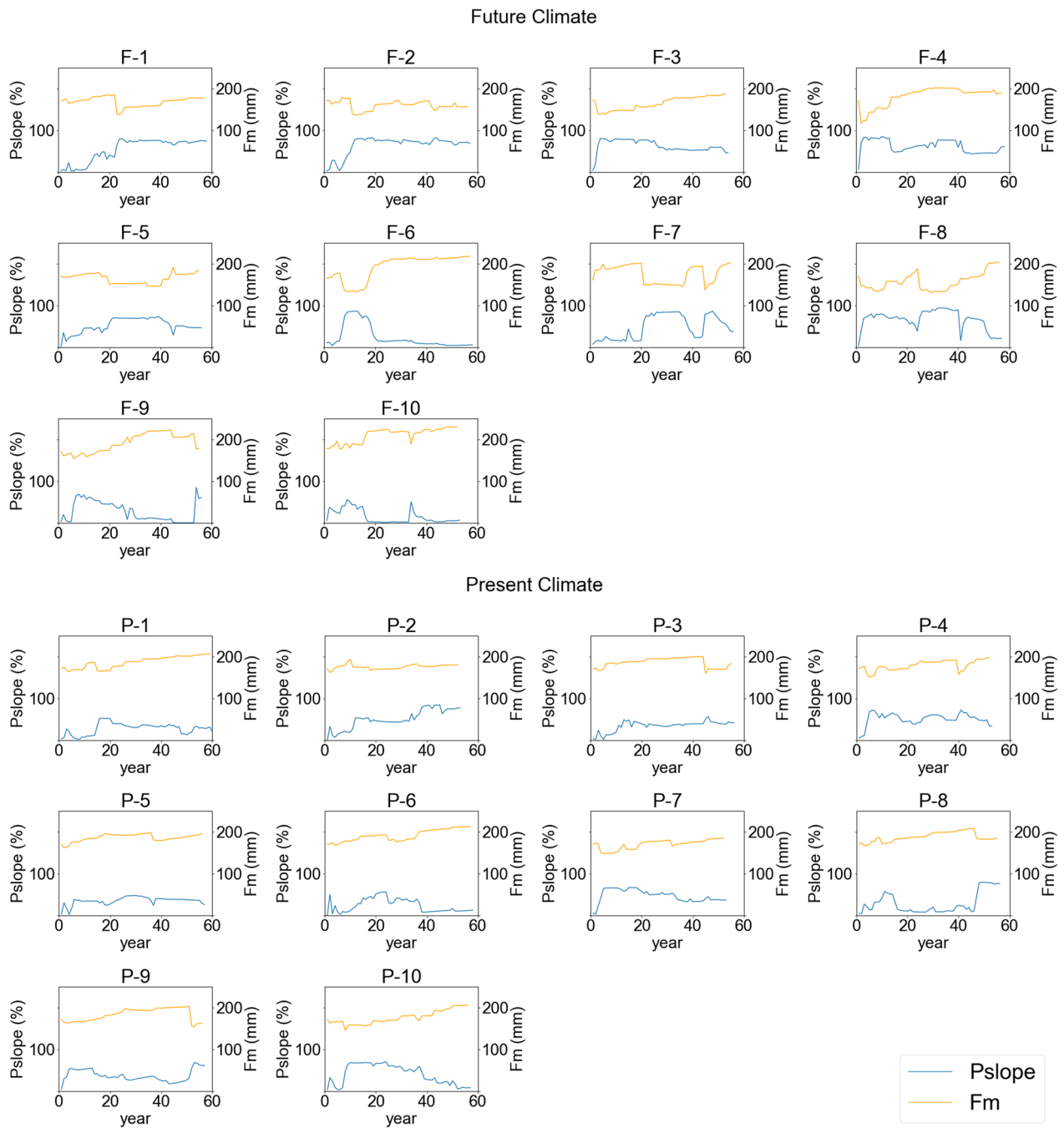
Fig. 8 The annual change over time in the proportion of sediment produced from the slope out of total sediment discharge (*Pslope*) per year for each member and the average grain size of the riverbed (*Fm*) at each end of the year
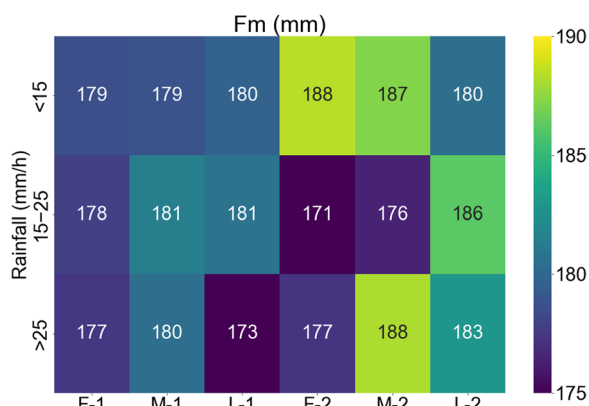
Fig. 9 The average grain size of the exchange layer averaged over all cases for each mesh. The horizontal axis represents the differences in rainfall patterns based on the clustering results shown in Fig. 4. The vertical axis represents the maximum rainfall by dividing it into three categories: 15 mm/h or less, more than 15 mm/h and 25 mm/h or less, and more than 25 mm/h

4 Discussion

The most significant aspect of this study was the statistical evaluation of future changes in sediment runoff using 600 years of projected climate change rainfall for each historical climate simulation and the +4 K future climate simulation. Although there have been previous studies on future changes in sediment discharge due to climate change, most of these analyses were based on a few rainfall patterns. For example, Lane et al. (2008) created three patterns of rainfall increase due to climate change (frequency, magnitude, and variability) and evaluated the change in discharge for each of these patterns. They obtained rainfall data for climate change, extending the observed rainfall in different ways for each rainfall

pattern, based on the ratio of the increase in peak flow in the A2 scenarios for the 2050s and the 2080s. Frequency change indicates that the number of days with rainfall increased, magnitude change indicates that rainfall increased equally on rainy days, and variability change indicates that rainfall increased on the three highest rainfall days. Their results showed that the volume of sediment discharge increased in all scenarios, with the pattern of increased frequency showing a smaller rate of increase than the other two patterns. However, in their study, future rainfall was established by processing the actual rainfall using monthly rainfall projections that were somewhat reliable. Therefore, no analyses have been conducted directly using hourly rainfall data from climate change projections. That is, it did not adequately account for the changes in rainfall patterns, as shown in Figs. 4 and 5. The reason behind this is because there is a problem with the reliability of the deterministic evaluation of sediment discharge by extracting a few patterns from the one-hour rainfall of climate change projections. To address this problem, we calculated the sediment discharge using 600 years of rainfall in a +4 K future climate

Table 5 The existence probability per annual maximum rainfall

Annual maximum rainfall (mm/h)	20 km		5 km	
	Present (P_{20})	Future (F_{20})	Present (P_5)	Future (F_5)
-15	96.0	86.8	76.5	60.6
15–25	4.0	12.0	17.7	23.0
25-	0.0	1.3	5.8	16.5

Table4 Rainfall and 10-day sediment discharge for each resolution

Return period	20 km		5 km		5 km/20 km	
	Present (P_{20})	Future (F_{20})	Present (P_5)	Future (F_5)	Present (P_5/P_{20})	Future (F_5/F_{20})
Annual maximum rainfall (mm/h)						
50	17.3	24.3	33.5	47.7	1.93	1.97
20	14.2	20.6	25.8	41.2	1.82	2.00
10	12.3	16.6	20.0	32.2	1.62	1.94
Total rainfall (mm/10 days)						
50	213.7	224.9	353.7	477.3	1.65	2.12
20	179.0	201.0	280.4	365.4	1.57	1.82
10	152.5	168.8	229.4	275.0	1.50	1.63
Amount of sediment discharge (m^3/10 days)						
50	5497	9288	52,107	152,833	9.48	16.45
20	2391	5560	23,965	87,747	10.02	15.78
10	1124	2218	7379	40,830	6.56	18.41

simulation and a historical climate simulation (1200 years in total) and treated the results statistically.

Our calculation results indicate that, in both the historical climate simulation and the +4 K future climate simulation, sediment from the channel bed is a greater source of production than sediment from the adjacent slope. However, there was a trend toward an increasing proportion of sediment from the slopes in the +4 K future climate simulation. This is consistent with the trend observed in the analysis conducted by Lane et al. (2008) for the Upper Wharfe catchment of Yorkshire Dales National Park in the U.K. Our results, which uses 1-h rainfall rates, also suggest that the frequency of short-duration rainfall events with high rainfall intensity will increase in the future, resulting in increased sediment production from slope failure. Jakob and Lambert (2009) stated that antecedent and short-term rainfall contributed to the temporal development of landslides in British Columbia, Canada, which supports the predictions of the soil moisture-dependent slope failure model employed in this study. However, Biasutti et al. (2016) investigated the relationship between past landslides and rainfall on the west coast of the USA and stated that the rainfall pattern that causes slope failure depends on the topography and climate. Therefore, further analysis of the relationship between rainfall patterns and slope failures is necessary.

When the grain size of the slope-failure sediment was finer than that of the channel bed, as in our study area, the mean grain size of the bed surface layer decreased with increasing slope failure. Egiazaroff (1965), Hirano (1971), and Buffington and Montgomery (1999) stated that the critical number of large gravel sheets decreases as fine sand is deposited on the riverbed, because the internal friction angle of the sediments (or bed surface roughness) decreases. Similar phenomena have been observed not only in gravel beds, but also in bedrock beds (Inoue et al. 2014; Mishra and Inoue 2020). The supply of sediment with a smaller grain size to the riverbed due to slope failure would have increased the transport capacity of the channel, and thus, the rate of future increase in sediment discharge would have been greater than that of rainfall.

A comparison of the sediment discharge calculated from rainfall data at 5 km and 20 km resolutions showed that the sediment discharge calculated from rainfall at 5 km resolution was significantly higher. This is because the 20-km resolution does not represent extreme rainfall events of short duration, as described by Rupa Kumar et al. (2006) and Westra et al. (2014). The bed shear stress must exceed the critical shear stress for the sediment in the riverbed to begin moving. As previously described, slope failure occurs when the water content of the soil exceeds a certain value. Thus, there is sufficient rainfall for sediment movement to occur, and the 20 km resolution of the rainfall data does not receive enough rainfall to exceed that amount, resulting in a very large difference in sediment discharge when compared at the same return period.

Finally, we present future challenges of the proposed model. In cold regions, such as the Pekerebetsu River basin, which is our study area, and in basins at high elevations, such as those in the Alps, sediment production by freezing and thawing is important, in addition to rainfall-induced slope failure (e.g., Gruber and Haeberli 2007). However, our model focuses on sediment production during heavy rainfall events and does not consider sediment production associated with temperature changes such as freezing and thawing. In general, if the temperature increases due to climate change, the frequency of freeze–thaw weathering is expected to decrease; however, it has been pointed out that in cold regions, the heat-retaining effect of snow cover may be lost, and the frequency of freeze–thaw events may increase (e.g., Rengers et al. 2020). In addition, increased evapotranspiration and flood frequency associated with climate change may contribute to bedrock weathering owing to wet-dry weathering (e.g., Sumner et al. 2022). It would be interesting to consider these effects in future studies.

5 Conclusions

Predicting changes in sediment discharge associated with future climate change is essential for assessing flood risk due to riverbed aggradation. To accurately predict sediment discharge, it is important to consider the effects of slope failure in mountainous areas and changes in grain size in mountain rivers on erosion and sediment transport. In this study, we investigated future changes in sediment production and discharge using a physics-based model that accounts for slope failure, channel erosion, and mixed grain-size sediment.

Our results indicate that future sediment discharge will be 3–5.5 times larger than the present sediment discharge, even though precipitation has increased only 1.2 1.6 times. Our results also show that the large increase in sediment discharge was caused by an increase in the frequency of slope failures owing to changes in rainfall patterns and an increase in the sediment transport capacity of mountainous channels by fine-grained sediment supplied from the slopes.

The amount of sediment discharge using 20 km resolution climate data is one order of magnitude smaller than that using 5 km resolution data, indicating that the 20 km resolution data cannot reproduce large-scale

Kido *et al. Progress in Earth and Planetary Science*   (2023) 10:54

Page 13 of 14

sediment discharge, such as the 2016 event. This is probably because climatic data with a 20 km resolution do not adequately reproduce topographical torrential rainfall in mountainous areas, and extreme events such as slope failures may not be accurately reproduced.

Abbreviations

LiDAR	Light detection and ranging
DEM	Digital elevation model
SiMHiS	Storm-induced multi-hazard information simulator
d4PDF	Database for policy decision making for future climate change

Supplementary Information

The online version contains supplementary material available at https://doi.org/10.1186/s40645-023-00580-0.

> **Additional file 1.** SiMHiS (Storm Induced Multi-Hazard Information Simulator).

Author contributions
TI conceived of the study. RK and KY conducted the experiments and drafted the figures. TI, MH, and KY contributed to the interpretation of the results. TI and MH supervised this study. RK drafted the manuscript with review, revision, and input from all authors. All the authors approved the final version of the manuscript.

Availability of data and materials
The datasets supporting the conclusions of this study are available at zenodo, https://doi.org/10.5281/zenodo.7549349.

Declarations

Competing interests
The authors declare that they have no competing interest.

References
Ahmed J, Constantine JA, Dunne T (2019) The role of sediment supply in the adjustment of channel sinuosity across the Amazon Basin. Geology 47:807–810. https://doi.org/10.1130/G46319.1

Alvioli M, Melillo M, Guzzetti F, Rossi M, Palazzi E, Von Hardenberg J, Brunetti MT, Peruccacci S (2018) Implications of climate change on landslide hazard in Central Italy. Sci Total Environ 630:1528–1543. https://doi.org/10.1016/j.scitotenv.2018.02.315

Aoki D, Kasai M, Igura M (2018) The effects of hydraulic structures on streams prone to bank erosion in an intense flood event: A case study from eastern Hokkaido. In: Symposium proceedings of the INTERPRAENENT 2018 in the Pacific Rim, pp 270–275

Ashida K, Egashira S, Liu B (1991) Numerical method on sediment sorting and bed variation in meander channels. Proc Hydraul Eng 35:383–390. https://doi.org/10.2208/prohe.35.383

Biasutti M, Seager R, Kirschbaum DB (2016) Landslides in west coast metropolitan areas: the role of extreme weather events. Weather and Climate Extremes. Sciencedirect 14:67–79. https://doi.org/10.1016/j.wace.2016.11.004

Buffington JM, Montgomery DR (1999) Effects of sediment supply on surface textures of gravel-bed rivers. Water Resour Res 35:3523–3530. https://doi.org/10.1029/1999WR900232

Ciabatta L, Camici S, Brocca L, Ponziani F, Stelluti M, Berni N, Moramarco T (2016) Assessing the impact of climate-change scenarios on landslide occurrence in Umbria Region, Italy. J Hydrol 541:285–295. https://doi.org/10.1016/j.jhydrol.2016.02.007

Cohen S, Syvitski J, Ashley T, Lammers R, Fekete B, Li H (2022) Spatial trends and drivers of bedload and suspended sediment fluxes in global rivers. Water Resour Res. https://doi.org/10.1029/2021WR031583

Creager WP, Justin D, Hinds J (1945) Engineering for dams, vol III. Wiley, New York, pp 645–649

Crozier M (2010) Deciphering the effect of climate change on landslide activity: a review. Geomorphology 124:260–326. https://doi.org/10.1016/j.geomorph.2010.04.009

Cunnane C (1978) Unbiased plotting positions—a review. J Hydrol 37:205–222. https://doi.org/10.1016/0022-1694(78)90017-3

Egiazaroff IV (1965) Calculation of nonuniform sediment concentrations. J Hydr Div 91:225–247. https://doi.org/10.1061/JYCEAJ.0001277

Furuichi T, Osanai N, Hayashi S, Izumi N, Kyuka T, Shiono Y, Miyazaki T, Hayakawa T, Nagano N, Matsuoka N (2018) Disastrous sediment discharge due to typhoon-induced heavy rainfall over fossil periglacial catchments in western Tokachi, Hokkaido, northern Japan. Landslides 15:1645–1655. https://doi.org/10.1007/s10346-018-1005-1

Gruber S, Haeberli W (2007) Permafrost in steep bedrock slopes and its temperature-related destabilization following climate change. J Geophys Res. https://doi.org/10.1029/2006JF000547

Hashimoto R, Tsuchida T, Moriwaki T, Kano S (2020) Hiroshima Prefecture geo-disasters due to western Japan torrential rainfall in July 2018. Soils Found 60:283–299

Hatono M, Yoshimura K (2020) Development of a global sediment dynamics model. Prog Earth Planet Sci 7:1–15. https://doi.org/10.1186/s40645-020-00368-6

Hirano M (1971) River-bed degradation with armoring. Proc Jpn Soc Civ Eng 1971:55–65. https://doi.org/10.2208/jscej1969.1971.195_55

Hokkaido Torrential Rainfall Hazard Research Team (2017) Hokkaido torrential rain disaster investigation team report (in Japanese)

Hoshino T, Yamada TJ (2023) Spatiotemporal classification of heavy rainfall patterns to characterize hydrographs in a high-resolution ensemble climate dataset. J Hydrol. https://doi.org/10.1016/j.jhydrol.2022.128910

Hürlimann M, Guo Z, Puig-Polo C, Medina V (2022) Impacts of future climate and land cover changes on landslide susceptibility: Regional scale modelling in the Val d'Aran region (Pyrenees, Spain). Landslides 19:99–118. https://doi.org/10.1007/s10346-021-01775-6

Inoue T, Nelson JM (2020) An experimental study of longitudinal incisional grooves in a mixed bedrock–alluvial channel. Water Resour Res. https://doi.org/10.1029/2019WR025410

Inoue T, Izumi N, Shimizu Y, Parker G (2014) Interaction among alluvial cover, bed roughness, and incision rate in purely bedrock and alluvial-bedrock channel. J Geophys Res Earth Surf 119:2123–2146. https://doi.org/10.1002/2014JF003133

Inoue T, Mishra J, Kato K, Sumner T, Shimizu Y (2020) Supplied sediment tracking for bridge collapse with large-scale channel migration. Water 12:1881. https://doi.org/10.3390/w12071881

Inoue T, Mishra J, Parker G (2021) Numerical simulations of meanders migrating laterally as they incise into bedrock. J Geophys Res Earth Surf. https://doi.org/10.1029/2020JF005645

IPCC (2021) The physical science basis. Contribution of Working Group I to the Sixth Assessment Report of the intergovernmental panel on climate change. In: Masson-Delmotte V et al (eds) Summary for policymakers. Climate change. Cambridge University Press, Cambridge, pp 3–32. https://doi.org/10.1017/9781009157896.001

Kido *et al. Progress in Earth and Planetary Science* (2023) 10:54

Page 14 of 14

Ishii M, Mori N (2020) d4PDF: Large-ensemble and high-resolution climate simulations for global warming risk assessment. Prog Earth Planet Sci 7:58. https://doi.org/10.1186/s40645-020-00367-7

Itakura T, Kishi T (1980) Open channel flow with suspended sediments. J Hydr Div 106:1325–1343. https://doi.org/10.1061/JYCEAJ.0005483

Jakob M, Lambert S (2009) Climate change effects on landslides along the southwest coast of British Columbia. Geomorphology 107:275–284. https://doi.org/10.1016/j.geomorph.2008.12.009

Lane SN, Tayefi V, Reid SC, Yu D, Hardy RJ (2007) Interactions between sediment delivery, channel change, climate change and flood risk in a temperate upland environment. Earth Surf Process Landf 32:429–446. https://doi.org/10.1002/esp.1404

Lane SN, Reid SC, Tayefi V, Yu D, Hardy RJ (2008) Reconceptualising coarse sediment delivery problems in rivers as catchment-scale and diffuse. Geomorphology 98:227–249. https://doi.org/10.1016/j.geomorph.2006.12.028

Li H, Tan Z, Ma H, Zhu Z, Abeshu WG, Zhu S, Cohen S, Zhou T, Xu D, Ruby LL (2022) A new large-scale suspended sediment model and its application over the United States. Hydrol Earth Syst Sci 26(3):665–688. https://doi.org/10.5194/hess-26-665-2022

Macqueen J (1967) Some methods for classification and analysis of multivariate observations. In: Berkeley symposium on mathematical statistics and probability 5, vol 1, pp 281–297

Métivier F, Lajeunesse E, Devauchelle O (2017) Laboratory rivers: Lacey's law, threshold theory, and channel stability. Earth Surf Dyn 5:187–198. https://doi.org/10.5194/esurf-5-187-2017

Milan DJ, Schwendel AC (2021) Climate-change driven increased flood magnitudes and frequency in the British uplands: geomorphologically informed scientific underpinning for upland flood-risk management. Earth Surf Process Landf 46:3026–3044. https://doi.org/10.1002/esp.5206

Ministry of Land, Infrastructure, Transport and Tourism (2017) Handouts for the 2nd technical review meeting on erosion control in the Tokachi river basin (in Japanese)

Mishra J, Inoue T (2020) Alluvial cover on bedrock channels: applicability of existing models. Earth Surf Dyn 8:695–716. https://doi.org/10.5194/esurf-8-695-2020

Miyazaki T, Sawada M, Matsuoka N, Tachikawa Y, Takashima S, Yoshida Y, Hayashi S, Furuichi T, Kasai M, Osanai N (2018) Large sediment discharge caused by periglacial slope failures and erosion induced by typhoon Lionrock (2016) in Pekerebetsu Creek, Hokkaido, Japan. JSECE J 71:22–33. https://doi.org/10.11475/sabo.71.2_22 (**in Japanese**)

Mizuta R, Murata A, Ishii M, Shiogama H, Hibino K, Mori N, Arakawa O, Imada Y, Yoshida K, Aoyagi T, Kawase H, Mori M, Okada Y, Shimura T, Nagatomo T, Ikeda M, Endo H, Nosaka M, Arai M, Takahashi C, Tanaka K, Takemi T, Tachikawa Y, Temur K, Kamae Y, Watanabe M, Sasaki H, Kitoh A, Takayabu I, Nakakita E et al (2017) Over 5,000 years of ensemble future climate simulations by 60-km global and 20-km regional atmospheric models. Bull Am Meteorol Soc 98:1383–1398. https://doi.org/10.1175/BAMS-D-16-0099.1

Peel MC, Finlayson BL, McMahon TA (2007) Updated world map of the Köppen–Geiger climate classification. Hydrol Earth Syst Sci 11(5):1633–1644. https://doi.org/10.5194/hess-11-1633-2007

Peres DJ, Cancelliere A (2018) Modeling impacts of climate change on return period of landslide triggering. J Hydrol 567:420–434. https://doi.org/10.1016/j.jhydrol.2018.10.036

Pitlick J, Mueller ER, Segura C, Cress R, Torizzo M (2008) Relation between flow, surface-layer armoring and sediment transport in gravel-bed rivers. Earth Surf Process Landf 33:1192–1209. https://doi.org/10.1002/esp.1607

Rachelly C, Vetsch DF, Boes RM, Weitbrecht V (2022) Sediment supply control on morphodynamic processes in gravel-bed river widenings. Earth Surf Process Landf 47:3413–3640. https://doi.org/10.1002/esp.5460

Rengers FK, Kean JW, Reitman NG, Smith JB, Coe JA, McGuire LA (2020) The Influence of frost weathering on debris flow sediment supply in an Alpine basin. J Geophys Res Earth Surf. https://doi.org/10.1029/2019JF005369

Rickenmann D, Koschni A (2010) Sediment loads due to fluvial transport and debris flows during the 2005 flood events in Switzerland. Hydrol Process 24:993–1007. https://doi.org/10.1002/hyp.7536

River Bureau, Ministry of Land, Infrastructure, Transport and Tourism (2006) Basic policy for river improvement of Tokachi River System River, Japan (in Japanese)

Rubey WW (1933) Settling velocities of gravel, sand, and silt particles. Am J Sci 25:325–338. https://doi.org/10.2475/ajs.s5-25.148.325

Rupa Kumar K, Sahai AK, Krishna Kumar K, Patwardhan SK, Mishra PK, Revadekar JV, Kamala K, Pant GB (2006) High-resolution climate change scenarios for India for the 21st century. Curr Sci Assoc 90(3):334–345

Shimizu M, Kanai S, Hotta N, Lissak C, Gomez C (2020) Spatial distribution of drifted-wood hazard following the July 2017 sediment-hazards in the Akatani river, Fukuoka Prefecture, Japan. For Geol 34:96–111. https://doi.org/10.23917/forgeo.v34i2.12434

Sklar LS, Dietrich WE (2004) A mechanistic model for river incision into bedrock by saltating bed load. Water Resour Res. https://doi.org/10.1029/2003WR002496

Sofia G, Nikolopoulos EI (2020) Floods and rivers: a circular causality perspective. Sci Rep 10:5175. https://doi.org/10.1038/s41598-020-61533-x

Sumner T, Mishra J, Inoue T, Shimizu Y (2022) Numerical study of the interaction between wet-dry weathering and bedload induced abrasion. Water Resour Res. https://doi.org/10.1029/2021WR030952

Tan Z, Leung LR, Li HY, Tesfa T, Zhu Q, Yang X, Liu Y, Huang M (2021) Increased extreme rains intensify erosional nitrogen and phosphorus fluxes to the northern Gulf of Mexico in recent decades. Environ Res Lett. https://doi.org/10.1088/1748-9326/abf006

Westra S, Fowler HJ, Evans JP, Alexander LV, Berg P, Johnson F, Kendon EJ, Lenderink G, Roberts NM (2014) Future changes to the intensity and frequency of short-duration extreme rainfall. Rev Geophys 52:522–555. https://doi.org/10.1002/2014RG000464

Wooding RA (1965) A hydraulic model for the catchment-stream problem: I. J Hydrol 3:254–267. https://doi.org/10.1016/0022-1694(65)90084-3

Yamada T, Hoshino T, Masuya S, Uemura F, Yoshida T, Omura N, Yamamoto T, Chiba M, Tomura S, Tokioka S, Sasaki H, Hamada Y, Nakatsugawa M (2018) The influence of climate change on flood risk in Hokkaido. Adv River Eng 24:391–396. https://doi.org/10.11532/river.24.0_391. (**in Japanese**)

Publisher's Note